Performance Analysis of a Hybrid Solar-Geothermal Power Plant in México

Eduardo González-Mora[1], Álvaro Lentz-Herrera[2] and Ma. Dolores Durán-García[1]

[1] Facultad de Ingeniería, Universidad Autónoma del Estado de México, Toluca (México)

[2] Programa de Energía, Universidad Autónoma de la Ciudad de México, Ciudad de México (México)

Abstract

Solar energy integration with existing geothermal power plants offers a promising approach to enhance renewable energy output. Hybrid systems, particularly those combining parabolic trough collectors (PTC) with geothermal facilities, can improve the efficiency and sustainability of energy production. This study investigates the feasibility of incorporating PTCs into the Cerro Prieto geothermal power plant to boost steam quality and increase overall energy generation. Specifically, we compared two configurations: using Therminol VP1 as the heat transfer fluid (HTF) and employing direct steam generation (DSG). Our results indicate that both configurations successfully enhanced steam quality, with VP1 showing higher exergy efficiency and requiring a smaller solar field area; DSG achieved superior energy efficiency but faced significant pressure drops. These findings demonstrate that solar-geothermal hybrid systems can significantly improve plant performance by carefully selecting the appropriate HTF and optimizing system parameters. This research underscores the potential of such hybrid systems to advance renewable energy technologies, providing valuable insights for future energy planning and policy development.

Keywords: Solar-geothermal hybrid systems, Parabolic trough collectors, Direct Steam Generation, Therminol VP1

1. Introduction

At the end of 2022, the global geothermal installed capacity was 16 318 MW, distributed across thirty-two countries. This value accounts for 0.16% of the world's total installed electric capacity, which stood at 10 216 390 MW (Ritchie and Rosado, 2023). In 2021, these countries generated 96,552 GWh of electricity from geothermal sources, representing 0.34% of global electric generation. Mexico ranks among the top ten countries with the highest geothermal capacity, occupying the sixth position behind New Zealand and Kenya, which have similar installed capacities.

Mexico's geothermal installed capacity totals 1 001.9 MW, consisting of thirty-nine power units across five geothermal fields. Most units are single and double-flash condensing types, collectively providing 924 MW. Fifteen backpressure units, each with a capacity of 5 MW, contribute a combined total of 75 MW. Additionally, two binary ORC units, each with a capacity of 1.45 MW and manufactured by Ormat, remain installed in Los Azufres, though they have been non-operational for several years. The largest flash plants, located in the Cerro Prieto field, each have a capacity of 110 MW, featuring two 55 MW turbines manufactured by Toshiba. Cerro Prieto is the oldest and largest geothermal field in the country.

Although installed capacity remained unchanged over the past three years, electric generation decreased by 16%, from 5 375 GWh to 4 511.5 GWh, in 2021. This decline resulted from the shutdown of two power units in 2021: Unit 1 of Cerro Prieto III, with a capacity of 110 MWe, and Unit 17 of Los Azufres, with a capacity of 53.4 MWe (Gutiérrez-Negrin et al., 2023). Net geothermal electric generation accounted for 1.3% of the total electric generation in Mexico in 2021, which was 323 527 GWh.

In 2021, the electricity generated within the Baja California electric grid, home to the Cerro Prieto power

Selection and/or peer review under responsibility of Scientific Committee
10.18086/eurosun.2024.07.07 Available at http://proceedings.ises.org

plants, amounted to 11 869.1 GWh. Of this, the geothermal units at Cerro Prieto generated 2 363.4 GWh, representing 19.9% of the total production. This isolated system, which includes major urban centers like Tijuana and Mexicali, relied on geothermal energy for its electricity needs, excluding self-supply, cogeneration, and imports from California, USA.

The Cerro Prieto geothermal field, owned by CFE (Comision Federal de Electricidad), is situated in northern Mexico, approximately 30 km south of the USA border, within the Ring of Fire. Spanning an area of approximately 20 km^2, with an additional 18 km2 allocated to the evaporation pond, Cerro Prieto comprises four distinct geothermal fields. Originally, Cerro Prieto I comprised five units with a total installed capacity of 180 MW. However, in 2011, four of these units, each with a capacity of 37.5 MW, were decommissioned, leaving only one operational unit with a capacity of 30 MW. Cerro Prieto II and III each boast a total installed capacity of 220 MW, powered by two identical units. The Cerro Prieto geothermal field encompasses more than 200 wells, varying in depth from 700 to 4,300 meters. At present, the installed capacity of the Cerro Prieto geothermal power plant amounts to 570 megawatts. The Cerro Prieto geothermal field features over 200 wells, with depths ranging from 700 to 4 300 m. Currently, the installed capacity of the Cerro Prieto geothermal power plant stands at 570 MW (Hernández Martínez et al., 2020).

In 2009, CFE proposed plans for Cerro Prieto V, a new plant comprising two 50 MW units, to increase Cerro Prieto's total capacity by 100 MW. However, following the earthquake in Mexicali in 2010, steam production was adversely affected, leading to the abandonment of the Cerro Prieto V project. Subsequently, with the permanent shutdown of the four Cerro Prieto I units in 2011, the geothermal field experienced a decline in steam production. Since then, CFE has been exploring various methods to augment energy generation.

The abundant solar radiation at Cerro Prieto, measured at 5.5 kW/m^2, surpassing the national average, presents a promising opportunity for solar energy utilization. In 2012, the installation of 5 MW power plants at Cerro Prieto incorporated four distinct technologies: polycrystalline panels with one and two-axis tracking systems, thin-film panels with a one-axis tracking system, and solar concentration panels with a two-axis tracking system. This initiative paved the way for a solar thermal plant to harness steam from wastewater discharged from the geothermal cooling towers, supplying steam to the Cerro Prieto pipeline grid for use in the steam turbines of the power plants. A water treatment facility must be installed to remove impurities from the blowdown before it enter the CSP plant and ensure the feedwater's quality (Miranda-Herrera, 2015).

2. Methodology

2.1. Overview for hybridization analysis

This study scrutinize the incorporation of commercial parabolic trough collectors (PTC) into the existing geothermal power plant Cerro Prieto to propose a solar-geothermal hybrid power plant. The hybridization looks to enhance the steam quality available in the geothermal wells as a function of the solar field size. To enhance the steam quality, we propose two configurations for the solar field employing two heat transfer fluids (HTF): thermal oil with a heat recovery steam generator (HRSG) and direct steam generation (DSG). For the thermal oil and HRSG (case 1), we use Therminol VP1 (VP1) as it is the standard HTF for solar power plants; while the DSG concept (case 2) employs the fluid available from the geothermal well. Both cases are shown in Fig. 1, while Table 1 depicts the geothermal well characteristics.

Tab. 1: Cerro Prieto geothermal well characteristics (Lentz and Almanza, 2006)

Parameter	Value
Pressure, (bar)	50
Temperature, (ºC)	263.9
Steam quality	0.2449
Mass flow rate, (kg/s)	46.17
Flash pressure, (bar)	10.5
Flash steam quality	0.3907

In México, Abengoa's successful deployment of the ASTR0 parabolic troughs (Fig. 2) in the integrated solar combined cycle Agua Prieta II informs the choice for the solar field, as this is the only CSP power plant in México. Table 2 summarizes the key parameters of the ASTR0 parabolic troughs.

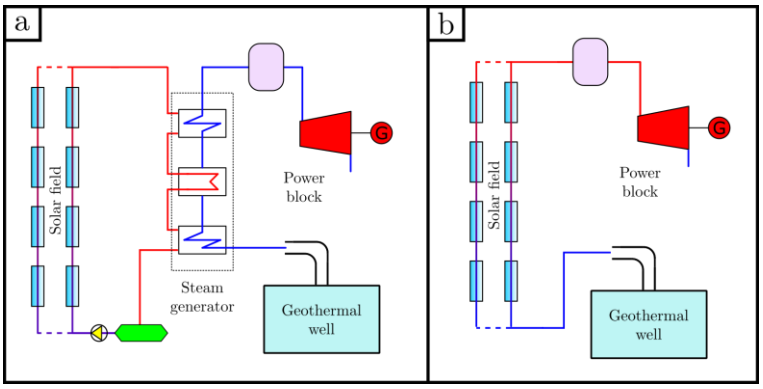

Fig. 1: Schematic diagram of the proposed systems for Cerro Prieto IV. (a) VP1 + HRSG (case 1). (b) DSG (case 2).

Tab. 2: Geometric parameters of the ASTR0 parabolic trough collector (ABENGOA, 2013)

Parameter	Value
Width, (m)	5.77
Focal length, (m)	1.71
Rim angle, (deg)	80.3
Receiver diameter, (m)	0.07

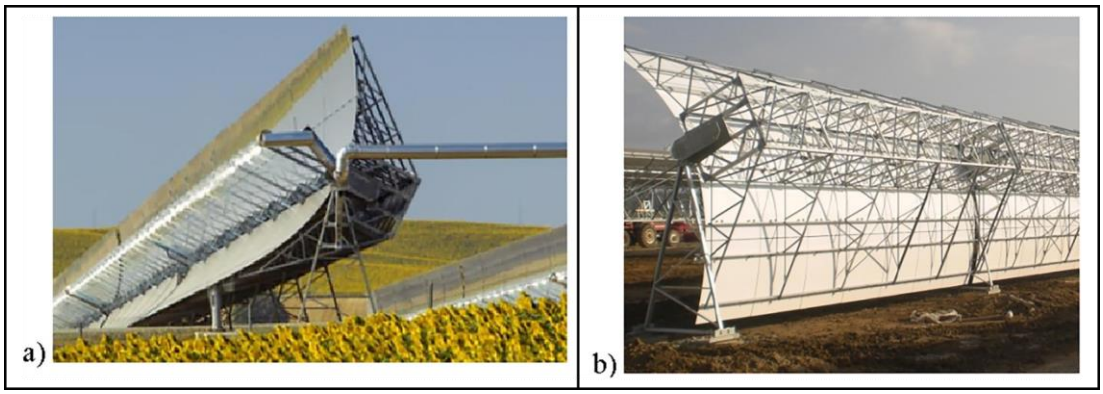

Fig. 2: Abengoa Solar ASTR0 collector (ABENGOA, 2013).

2.2. Evaluation procedure

Fig. 3. illustrates the calculation procedure for assessing the solar fields. The initial step involves the definition of the steam quality enhancement of the geothermal fluid before the flashing process. Following this determination, we proceed with the thermohydraulic characterization of the solar fields, which in this study, encompass PTC with VP1 and DSG. After analysing these solar fields setups, we consolidate the results into 5 functions that allow the evaluation as a function of the solar field size. These functions encompass:

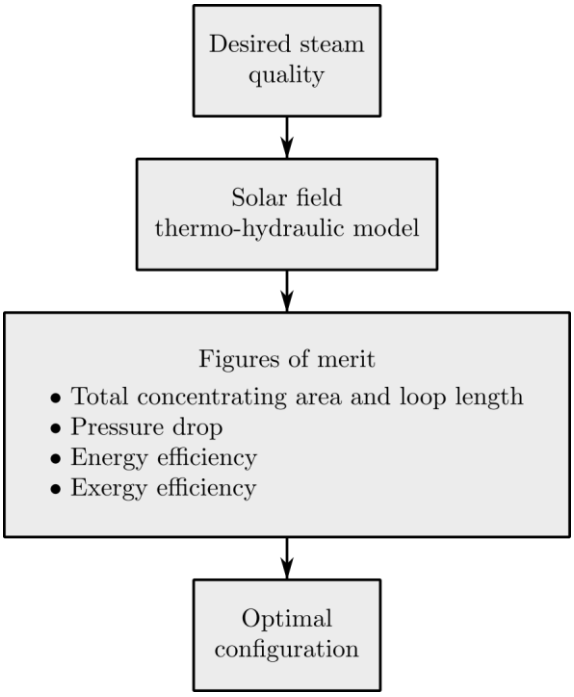

Fig. 3: Evaluation procedure.

- Steam quality enhancement: Increasing the quality of the stem delivered to the turbine is the main objective of the study. This process will be attained using the solar radiation to heat Therminol VP1 and a HRSG, or the DSG concept. One can define the desired steam quality and compute the thermal load to be delivered by the solar field:

$$\dot{Q}_{gain,HTF} = \dot{m}_{HTF}\left(h_{out,SF} - h_{in,SF}\right) \qquad \text{(eq. 1)}$$

- Total concentrating area and loop length: The loop size depends on the desired quality to be attained for the steam turbine. To determine the concentrating area they loop lengths are considered for mirror placement. In this study, the total concentrating area is solely associated with the mirrors, accounting the loops number N_{loop}, loop's length (L_{loop}) and the PTC width (W_{PTC}), as:

$$A_{SF} = N_{loop} L_{loop} W_{PTC} \qquad \text{(eq. 2)}$$

The loops number is determined by the mass flow rate within the receiver. It is suggested to maintain a turbulent flow (Re~10^5) to ensure efficient heat transfer between the receiver tube and the HTF.

- Pressure drop. Longer loops led to higher pressure drop, limited by the desired pressure in the flash tank to deliver the steam at the steam turbine. In the case of VP1, the pressure drop must be carefully traced to avoid any phase change.
- Energy and exergy efficiency: The solar field's energy efficiency can be evaluated by comparing the net thermal power transferred to the heat transfer fluid ($\dot{Q}_{gain,HTF}$) to the incident solar power on the net mirror area ($\dot{Q}_{inc}$). This calculation provides insight into the conversion of solar energy into usable thermal power, expressed as:

$$\eta_{I,SF} = \frac{\dot{Q}_{gain,HTF}}{\dot{Q}_{inc}} = \frac{\dot{m}_{HTF}\left(h_{out,SF} - h_{in,SF}\right)}{A_{SF} G_{bn}} \qquad \text{(eq. 3)}$$

The exergy efficiency of the solar field can be computed as the ratio of the fluid exergy increment ($\dot{E}x_{gain,HTF}$) to the exergy of solar radiation incident on the net mirror area ($\dot{E}x_{inc}$). This parameter provides insight into the solar field's effectiveness in transforming solar radiation into practical exergy in the form of thermal power, expressed as:

$$\eta_{II,SF} = \frac{\dot{E}x_{gain,HTF}}{\dot{E}x_{inc}} = \frac{\dot{m}_{HTF}(ex_{out,SF} - ex_{in,SF})}{A_{SF}\dot{E}x_{G_{bn}}} \quad \text{(eq. 4)}$$

The exergy associated with solar radiation has been extensively discussed in the literature, leading to different models and approaches to estimate it. Recently, researchers have made a progress in an improved model, addressing shortcomings in existing approaches (González-Mora et al., 2023). The model integrate the principles of endoreversible thermodynamics, accounting for external irreversibilities within the solar collector system. The exergy of solar radiation can be expressed as follows:

$$\dot{E}x_{G_{bn}} = G_{bn}\left[1 - \frac{1}{\xi}\left(\frac{T_a}{T_{sun}}\right)^4\right]\left(1 - \frac{\lambda_c T_0}{\lambda_c T_a + \xi\sigma T_{sun}^4 - \sigma T_a}\right) \quad \text{(eq. 5)}$$

where T_{sun} is the equivalent absolute temperature of the sun as a black-body (~5800 K), T_0 is the ambient temperature, ξ is the concentration acceptance product, λ_c is the thermal conductance per unit surface area of the environment, and σ is the Stefan-Boltzmann constant. The value of T_a is the solution of $\mathrm{d}\dot{E}x_{G_{bn}}/\mathrm{d}T_a = 0$. It can be demonstrated that in the limit case, Eq. 5 takes a value of $\dot{E}x = 0.8391AG_{bn}$ (González-Mora et al., 2023).

For the solar field using VP1 as HTF, the energy and exergy efficiency must consider the proper HRSG efficiency. The HRSG efficiencies can be determined considering the $T - \dot{Q}$ diagram in Fig. 4, and the total efficiency values are calculated as:

$$\eta_I = \eta_{I,SF}\eta_{I,HRSG} \quad \text{(eq. 6)}$$

$$\eta_{II} = \eta_{II,SF}\eta_{II,HRSG} \quad \text{(eq. 7)}$$

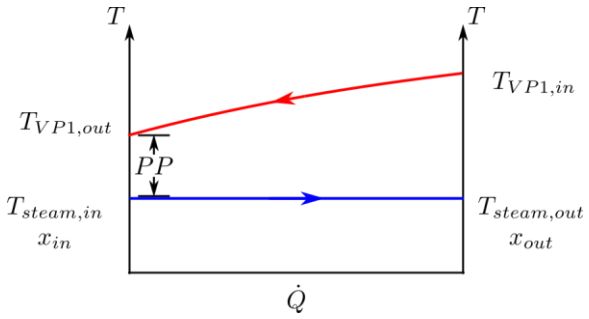

Fig. 4: Heat recovery steam generator $T - \dot{Q}$ diagram.

2.3. Details on solar field's thermohydraulic model

The present model employs the 'Homogeneous Equilibrium Model' approach with a 1D finite difference method, as described and validated by González-Mora and Durán-García (2023, 2024).The model applies a steady-state energy balance over the receiver (heat collector element, HCE), considering the direct normal solar irradiation, optical losses, thermal losses, and HTF gains. Unlike other models, the present model does not rely on the convective heat transfer coefficient (h) and the friction factor (f), enabling a faster computation time as no iterative processes are required to characterize the solar field. Fig. 5 displays the HCE for the parabolic trough, while Eqs. 8 shows the balance equations per unit length.

$$\begin{cases} \dot{q}'_{12,conv} = \dot{q}'_{23,cond} \\ \dot{q}'_{3,SolAbs} = \dot{q}'_{34,conv} + \dot{q}'_{34,rad} + \dot{q}'_{23,cond} + \dot{q}'_{38,cond} \\ \dot{q}'_{45,cond} = \dot{q}'_{34,conv} + \dot{q}'_{34,rad} \\ \dot{q}'_{45,cond} + \dot{q}'_{5,SolAbs} = \dot{q}'_{56,conv} + \dot{q}'_{57,rad} \\ \dot{q}'_{12,conv} = \frac{\dot{m}}{L_{HCE}}(h_{in} - h_{out}) \end{cases} \quad \text{(eq. 8)}$$

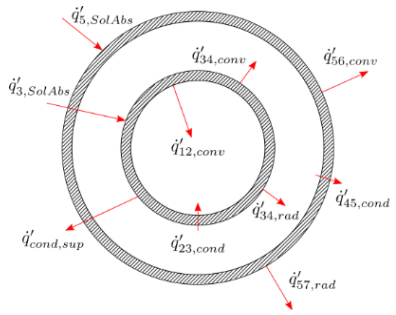

1. HTF
2. Absorber tube inner surface
3. Absorber tube external surface
4. Glass cover inner surface
5. Glass cover outer surface
6. Environment
7. Sky

Fig. 5: Heat fluxes over the PTC receiver. Adapted from (González-Mora and Durán-García, 2024)**.**

The Eqs. 8 simplifies the absorption in the receiver and the glass cover as surface phenomena. In addition, it is assumed that temperatures, heat flows and thermodynamic properties are uniform in the whole cross section area. In this regard, one can express each heat flow as:

$$\begin{cases} \dot{q}'_{i,SolAbs} = IAM\rho_{PTC}(\alpha\tau)_i W G_{bn} \\ \dot{q}'_{ij,cond} = \frac{2\pi k_{ij}(T_i - T_j)}{\ln D_j/D_i} \\ \dot{q}'_{ij,rad} = \frac{\sigma\pi D_i\left(T_i^4 - T_j^4\right)}{\frac{1}{\varepsilon_i} + \frac{(1-\varepsilon_j)D_i}{\varepsilon_j D_j}} \\ \dot{q}'_{ij,conv} = f(\Delta T) \end{cases} \quad \text{(eq. 9)}$$

where IAM represents the incidence modifier angle, ρ_{PTC} is the mirror reflectance, $(\alpha\tau)_i$ is the product of the absorbance and transmittance of surface i, W_{PTC} is the PTC width, G_{bn} is the incident solar radiation in the normal direction, k is the surface conductivity, T is the temperature, D is the diameter, σ is the Stefan-Boltzmann constant, ε is the emittance. The subscripts i and j are used to identify each of the surfaces, as shown in Fig. (4b). It is important to note that the last equation in the set of Eqs. (9) implies a functional of the temperatures, for the purpose of avoiding the use of the convective coefficient.

To model the annulus between the absorber tube and the glass cover, free convection between two cylinders is considered, since the receiver is evacuated. The convection between the glass cover and the environment can be forced or natural, depending on the atmospheric conditions; for natural convection, the Churchill and Chu equation is used, while for forced convection the Žhukauskas equation is applied. Regarding convection between the absorber tube and the heat transfer fluid, there are two scenarios: the Pethukhov or Gnielinski equation for single-phase flow and the Gungor and Winterton correlation for two-phase flow.

For the DSG case, the flow pattern inside the receiver must be taken into account. It is suggested that PTC under DSG should operate within the annular-flow pattern (Zarza Moya, 2003) to enhance the heat transfer rate, avoid thermal stresses and attain higher efficiency. Consequently, we rely on the Taitel and Dukler diagram (1976) to characterize the flow pattern due to its ease of use, and high accuracy.

3. Results and discussion

The evaluation of the whole model is performed in an inhouse code. The flow from the wells has a low

concentration of salts (<2%); for this reason, it is possible to assume that the geothermal fluid behaves as water (Lentz and Almanza, 2006). In both proposed systems, solar field with VP1 and DSG, the steam quality enhancement after the flashing is modelled until reaching the saturated vapor condition, so the solar field, and the HRSG, should attain a steam quality of 0.9894 before the flashing. Doing this, we can retrieve the upper performance limits that will allow projections of several configurations for the geothermal power plant.

3.1. General considerations

A heat demand of 57.27 MW to be supplied to the geothermal fluid to attain the desired steam quality enhancement of saturated vapor. This heat demand must be supplied by the solar field, either with VP1 or DSG, respectively.

We fix some values regarding the VP1 in the steam generator, namely the temperature at the HSRG ($T_{VP,1}$) inlet and the pinch point (PP). We define $T_{VP,1}$ at 390ºC and PP at 20ºC and their pressure at 12 bar, to avoid any phase change of thermal oil. Applying an energy balance for the HRSG (see Fig. 4), recalling that $x_{in} = 0.2449$, $x_{out} = 0.9894$, and a pressure drop of 3 bar in both fluids, a typical value present in HRSG of CSP plants (Lippke, 1995).

Under these considerations, 208.3 kg/s of VP1 is required to meet the requirements. As stated in Section 2.2, a turbulent flow must be attained in the receiver. Consequently, we select 125 loops, each one with 1.667 kg/s flowing in the receiver tube with a Reynolds number high enough to keep a turbulent flow. With the VP1 thermal conditions, a 90.97% energy efficiency ($\eta_{I,HRSG}$) and 92.07% exergy efficiency ($\eta_{II,HRSG}$) are expected in the HRSG. For the DSG solar field, the 46.17 kg/s are distributed between 20 loops, with 2.308 kg/s per loop. This mass flow rate allows a proper annular flow as shown below.

3.2. Solar field behaviour

As stated in Section 2.2, we define four parameters to characterize the upper limits for the steam quality enhancement requirements related to the solar field (and the HRSG for VP1). These parameters define our figures of merit that relates loop size (and total concentrating area), pressure drop, energy efficiency and exergy efficiency. These figures of merit are plotted in Fig. 6.

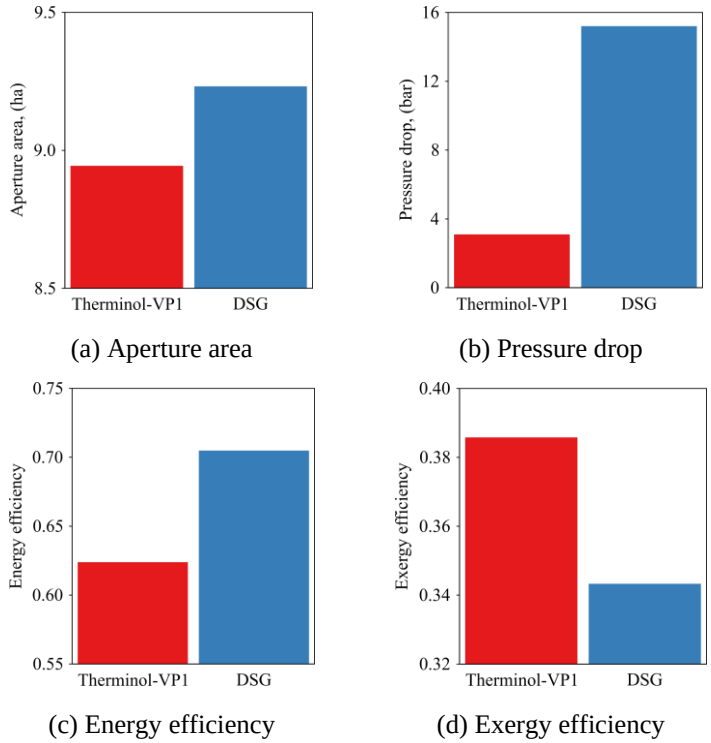

(a) Aperture area (b) Pressure drop

(c) Energy efficiency (d) Exergy efficiency

Fig. 5: Figures of merit

From Fig. 6, comparing VP1 and DSG, distinct differences in key performance metrics are retrieved. The area

required for VP1 is slightly smaller at 8.944 hectares compared to 9.232 hectares for DSG. However, the DSG configuration necessitates a significantly longer length of 796 meters, in contrast to the 120 meters required for Therminol VP1. When evaluating energy efficiency, DSG demonstrates a superior efficiency of 0.7049, surpassing VP1 efficiency of 0.6239. Conversely, VP1 exhibits higher exergy efficiency at 0.3858, while DSG registers a lower exergy efficiency of 0.3433. A notable distinction is observed in the pressure drop; DSG experiences a substantial pressure drop of 15.2 bar, whereas VP1 records a markedly lower pressure drop of 3.1 bar. It is important to note that the pressure drop for Therminol VP1 already includes the pressure drop in the HRSG. The low exergy value obtained in the DSG, stands for the high pressure drop along the loops. These results underscore the trade-offs between the two configurations, highlighting DSG's higher energy efficiency at the expense of greater pressure drop and area requirements, while Therminol VP1 offers a more compact and thermodynamically favorable alternative since the exergy efficiency is higher.

Upon characterizing the DSG in the solar field, we constructed the Taitel and Dukler diagram (Fig. 7) to identify the flow pattern inside the receiver tube. The operating conditions of pressure and mass flow rate ensured an annular flow throughout the entire boiling process, despite the high-pressure drop. This indicates that the boiling process can proceed without major complications, providing confidence in the system's operational stability and effectiveness.

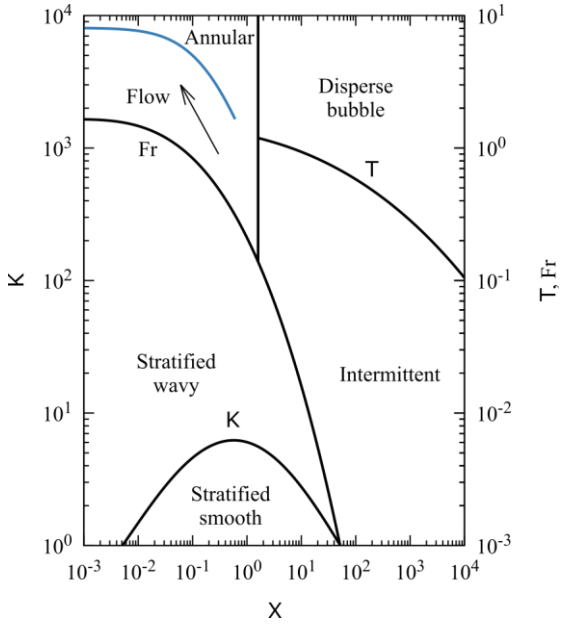

Fig. 7: Boiling process flow pattern

4. Conclusions

This study evaluated the feasibility of integrating parabolic trough collectors (PTC) with the Cerro Prieto geothermal power plant to enhance steam quality and increase energy production. The research focused on two configurations: using Therminol VP1 as the heat transfer fluid (HTF) and employing direct steam generation (DSG). We aimed to determine which configuration could effectively augment the geothermal plant's efficiency and output.

The study highlights the significant potential of solar-geothermal hybrid systems. Compared to DSG, using VP1 required a slightly smaller solar field area, demonstrating higher exergy efficiency. Conversely, DSG achieved superior energy efficiency but faced a considerable pressure drop. These results underscore the trade-offs between the two approaches regarding efficiency and operational challenges, indicating that both have distinct advantages and limitations depending on the specific operational goals and conditions.

The study demonstrated that both configurations could enhance steam quality to the desired levels, proving the concept's viability. The findings provide valuable insights into the performance metrics of hybrid solar-geothermal power plants, emphasizing the importance of selecting the appropriate HTF and optimizing system

parameters. In addition, the study confirmed that integrating PTCs into geothermal plants could significantly improve their performance, thus validating the potential for such hybrid systems.

PTC integration improves steam quality and offers a pathway to increase renewable energy output in regions with abundant solar resources. The enhanced steam quality can lead to higher electricity generation efficiency, making hybrid plants more competitive and reducing dependency on fossil fuels. This research sets a foundation for policymakers and industry stakeholders to consider hybrid solutions in future energy planning and development. Future research should explore long-term operational impacts, cost-benefit analysis, and scalability of the proposed hybrid systems. In addition, investigating other HTFs and advanced materials for PTCs could further optimize system performance and economic viability.

5. References

ABENGOA, 2013. A new generation of parabolic trough technology.

González-Mora, E., Durán-García, M.D., 2024. Alternative Approach for Thermo-Hydraulic Modeling of Direct Steam Generation in Parabolic Trough Solar Collectors. J Therm Sci Eng Appl 16, 1–12. https://doi.org/10.1115/1.4064819

González-Mora, E., Durán-García, M.D., 2023. Alternative Methodology for Modeling Direct Steam Generation in Parabolic Collectors: A Study Case in Northeast Mexico, in: 36th International Conference on Efficiency, Cost, Optimization, Simulation and Environmental Impact of Energy Systems (ECOS 2023). ECOS 2023, Las Palmas De Gran Canaria, Spain, pp. 1496–1506. https://doi.org/10.52202/069564-0136

González-Mora, E., Poudel, R., Durán-García, M.D., 2023. A practical upper-bound efficiency model for solar power plants. Journal of Non-Equilibrium Thermodynamics. https://doi.org/10.1515/jnet-2022-0080

Gutiérrez-Negrin, L., Izquierdo-Montoya, G., Canchola-Félix, I., 2023. Situation of geothermal energy in Mexico: country update, in: Proceedings of the World Geothermal Congress 2023. Beijin.

Hernández Martínez, E., Avitia Carlos, M.C.P., Cisneros Solís, J.I., Prieto Avalos, M.C.M. del C., 2020. Thermodynamic simulation and mathematical model for single and double flash cycles of Cerro Prieto geothermal power plants. Geothermics 83, 101713. https://doi.org/10.1016/j.geothermics.2019.101713

Lentz, Á., Almanza, R., 2006. Solar–geothermal hybrid system. Appl Therm Eng 26, 1537–1544. https://doi.org/10.1016/j.applthermaleng.2005.12.008

Lippke, F., 1995. Simulation of the part-load behavior of a 30 MWe SEGS plant. Sandia National Lab.(SNL-NM), Albuquerque, NM (United States).

Miranda-Herrera, C., 2015. Power Generation in Cerro Prieto Geothermal Field, in: World Geothermal Congress . Melbourne.

Ritchie, H., Rosado, P., 2023. Data Page: Geothermal energy capacity" [WWW Document]. Energy. URL https://ourworldindata.org/grapher/installed-geothermal-capacity (accessed 5.26.24).

Taitel, Y., Dukler, A.E., 1976. A model for predicting flow regime transitions in horizontal and near horizontal gas-liquid flow. AIChE Journal 22, 47–55. https://doi.org/10.1002/aic.690220105

Zarza Moya, E., 2003. Generación directa de vapor con colectores solares cilindro parabólicos. Proyecto DIrect Solar Steam (DISS). Universidad de Sevilla.